Polymer Degradation and Stability 197 (2022) 109872

Contents lists available at ScienceDirect

Polymer Degradation and Stability

journal homepage: www.elsevier.com/locate/polymdegradstab

Influence of photooxidation on ionic reversible interactions of ionic poly(ether urethane)/silica hybrids

J.-E. Potaufeux[a,b], G. Rapp[c], S. Barrau[d], G. Liu[e], C. Zhang[e], Emmanuel P. Giannelis[f], D. Notta-Cuvier[b], F. Lauro[b], J.-M. Raquez[a], J. Odent[a,*], S. Therias[c,*]

[a] Laboratory of Polymeric and Composite Materials (LPCM), Center of Innovation and Research in Materials and Polymers (CIRMAP), University of Mons (UMONS), Place du Parc 20, 7000 Mons, Belgium
[b] Laboratory of Industrial and Human Automatic Control and Mechanical Engineering (LAMIH), UMR CNRS 8201, University Polytechnique Hauts-De-France (UPHF), Le Mont Houy, 59313, Valenciennes, France
[c] Université Clermont Auvergne, CNRS, Clermont Auvergne INP, ICCF, F-63000 Clermont-Ferrand, France
[d] Université de Lille, CNRS, INRAE, Centrale Lille, UMR 8207 - UMET - Unité Matériaux et Transformations, F-59000 Lille, France
[e] Beijing National Laboratory for Molecular Sciences, CAS Key Laboratory of Engineering Plastics, Institute of Chemistry, Chinese Academy of Sciences, Beijing 100190, China
[f] Department of Materials Science and Engineering, Cornell University, Ithaca, NY 14853, USA

ARTICLE INFO

Article history:
Received 15 November 2021
Revised 2 February 2022
Accepted 16 February 2022
Available online 18 February 2022

Keywords:
Ionic nanocomposite
Dynamic bonding
Poly(ether urethane)/silica hybrid
Photooxidation
Accelerated environmental ageing

ABSTRACT

Organic-inorganic hybrids that combine the reversible nature of electrostatic interactions present in ionic systems with the reinforcement ability of nanoparticles in nanocomposites have the potential to revolutionize a wide spectrum of technologies. However, the prediction of their service lifetime under photooxidative conditions has remained elusive. In this paper, the accelerated environmental ageing of ionic hybrid materials made by combining imidazolium-functionalized poly(ethylene glycol)-based polyurethane (*im*-PU) and surface-modified sulfonate silica nanoparticles (SiO_2-SO_3H) is addressed. Since the resulting ionic nanocomposites are dynamic, the present contribution aims to elucidate their temporal behavior and precisely distinguish the contribution of the nanoparticles addition to the photochemical behavior. Although the addition of SiO_2-SO_3H nanoparticles within *im*-PU matrix led to faster photooxidative degradation, the ionic imidazolium-sulfonate crosslinks are thought to be sustained under photooxidative conditions. The results further suggest that the molecular weight loss and the resulting ductile-to-brittle transition for the ionic hybrid under atmospheric ageing conditions are attributed to severe chain scissions into the *im*-PU backbone in the presence of SiO_2-SO_3H nanoparticles. Overall, the present investigation suggests that the silica nanoparticles addition is responsible for the prodegradant effect rather than the presence of reversible ionic interactions in the system. The present work thus provides a deeper understanding about the crucial role of the incorporation of dynamic linkages within ionic nanocomposites during photochemical ageing and can aid the future design and use of these systems.

1. Introduction

Dynamic polymeric materials, whereby specific bonds or interactions can undergo reversible breaking and restoration under certain conditions have gained significant attention and opened up new pathways for the design of tunable adaptive materials [1–3]. Among these dynamic polymer systems, ionic materials leverage the dynamic and reversible nature of electrostatic bonding by maximizing Coulomb interactions in the system [4–6]. Yuan *et al.* recently designed ionic hydrogels made of a mixture of two polycations and two polyanions of different acid dissociation constant, resulting in unique mechanical performance (*i.e.* enhanced toughness and stiffness) and self-healing characteristics [7]. Meanwhile, the growing interest in nanoparticles led to the development of ionic organic-inorganic hybrids based on surface-modified nanoparticles. These dynamic systems demonstrated how combining the dynamic and reversible nature of electrostatic interactions present some advantages with the reinforcement ability of nanoparticles [8–11]. In addition, our group recently designed multi-responsive ionic nanocomposites made of poly(ethylene glycol)-based polyurethanes with pendant imidazolium cationic sites (*im*-PU) and anionic surface-modified sulfonate silica nanoparticles (SiO_2-SO_3H) that combine simultaneous improvement in stiffness, toughness and ductility [8]. In addition to their exceptional mechanical performance, these ionic nanocom-

* Corresponding authors
E-mail addresses: jeremy.odent@umons.ac.be (J. Odent), sandrine.therias@uca.fr (S. Therias).
https://doi.org/10.1016/j.polymdegradstab.2022.109872
0141-3910/

posites exhibit unique strain-dependent behavior (*i.e.* the deformation increases with increasing strain rate) and returns to original state after deformation integrating shape-memory with self-healing behaviors. The materials performance was attributed to the dynamic and reversible nature of the ionic imidazolium-sulfonate interactions present in the system. Further introducing these ionic moieties with a biosourced polylactide (PLA) through melt-blending also endowed the final material with ultra-toughness [9]. Ionically modified silica nanoparticles are thought to play a crucial role in these systems by creating multiple temporary ionic crosslinks between polymer chains, thus governing the overall material performance. More recently, we proposed that the origin of the underlying mechanisms governing the superior performance is based in the ionic nature of the organic-inorganic hybrids, and was attributed to the dissociation dynamics of the ionic crosslinks.

Depending on the targeted application, these materials can be exposed to environmental ageing factors that include temperature and humidity variations as well as solar light exposure, which ultimately influence the degree of ageing together with the performance level of the end product under normal-usage conditions [12]. Specifically, UV light irradiation causes photooxidative degradation, which can result in deterioration of the overall properties of materials at every scale. Despite the growing interest in nanocomposites, the effect of the presence of nanofillers on the photochemical ageing and durability features is hardly predictable [13]. The photodegradation stability of (nano)composites depends on the nature of the (nano)particles, leading to improved ageing resistance in several systems [14–20], while being prodegradant in other systems [21,22]. Although a significant acceleration of ageing could result from the possibly altered segmental dynamics close to the particle-matrix interface through (nano)particle surface functionalization [23–26], such a variable has been hardly investigated. Very few studies address the issue of ageing on high-performance ionic materials, resulting so far in *e.g.* a drop of conductivity for polyelectrolytes containing lithium salts [27], or a ductile-to-brittle transition for ethylene-based ionomers [28] under atmospheric ageing conditions. As long-term performance and durability are critical in technological development of novel materials, deeply understanding the responsible mechanism(s) related with the age-based changes is thought to play a crucial role in predicting the reliable lifetime of such advanced materials under realistic in-use conditions.

In the present study, we elucidate the mechanism and propose a fundamental understanding of the photodegradation behavior of ionic organic-inorganic hybrids made of imidazolium-functionalized poly(ethylene glycol)-based polyurethanes

(*im*-PU) and surface-modified sulfonate silica nanoparticles (SiO_2-*SO_3H*). The present work relies on a systematic study of the chemical modifications and degradation kinetics through Fourier transform infrared spectroscopy (FTIR) as well as the thermal, mechanical and morphology alterations of the ionic hybrids in comparison with neat *im*-PU in photooxidative conditions. We also distinguish contributions of the silica nanoparticle addition towards the dissociation dynamics of electrostatic interactions present in such high-performance ionic systems through photochemical ageing. This work permits in-depth understanding of the accelerated environmental ageing of ionic hybrid materials, which should inspire others and lead to novel ionic polymeric materials with long-term performance and durability.

2. Material & methods

2.1. Materials

Polyethylene glycol (PEG, 2000 g.mol^{-1}, Alfa Aesar), 2,2-bis(bromomethyl)propane-1,3-diol (BBPDO, 98%, Sigma), 1-methylimidazole (99%, Aldrich), dibutyltin dilaurate (DBTDL, 95%, Sigma), Ludox HS30 colloidal silica (mean diameter 18 nm, Aldrich), 3-(hydroxysilyl)-1-propane sulfonic acid (SIT, 40 wt%, Gelest), sodium hydroxide solution (1M, Aldrich), anhydrous tetrahydrofuran (THF, >99.8%), anhydrous *N,N*-dimethylformamide (DMF, >99.7%, Alfa Aesar), diethyl ether (>99%, Aldrich) were used without further purification. Hexamethylene diisocyanate (HMDI, >98%, Aldrich) was stored in a glove box.

2.2. Design of ionic nanocomposites

Imidazolium-functionalized poly(ethylene glycol)-based polyurethane (*im*-PU, $M_n \approx 58{,}000$ g.mol^{-1}, $Đ \approx 1.9$, yield ≈ 95%) and surface-modified sulfonate silica nanoparticles (SiO_2-*SO_3H*, *ca.* 17 ± 5 nm of diameter, 1 ± 0.1 mmol of SO_3H/g of silica) were prepared according to a previously reported procedure [8]. Briefly, *im*-PU of *ca.* 0.1 mmol.g^{-1} of imidazolium moieties was synthesized by the reaction of 1.2 eq. of hexamethylene diisocyanate with 0.9 eq. of polyethylene glycol oligomer, 0.1 eq. of imidazolium-based diol and catalytic amounts of dibutyltin dilaurate in anhydrous DMF at 60°C for 6 h under nitrogen. The resulting *im*-PU was then recovered by precipitation into a 10-fold excess of diethylether, followed by filtration and drying under vacuum. SiO_2-*SO_3H* of *ca.* 1 mmol of SO_3H/g of silica was prepared by adding 3-(trihydroxysilyl)-1-propanesulfonic acid into a colloidal silica suspension, while stirring vigorously. The suspension was then heated to 70°C under stirred for 24 h and subsequently dialyzed against deionized water for 3 days while changing the water twice a day. The as-synthesized *im*-PU was dissolved in deionized water followed by the dropwise addition of 10 wt% of sulfonate silica suspension under stirring, sonication and freeze-drying to form ionic *im*-PU/SiO_2-*SO_3H* hybrids. The resulting materials were shaped into films of 300 μm by compression molding at 60°C under 10 bars using a CARVER machine with the following sequence: no pressure for 2 minutes followed by 3 degassing steps and 1 minute under 10 bars.

2.3. Photochemical ageing

Photodegradation experiments were conducted using a Suntest CPS/XLS Atlas device, equipped with an ATLAS (NXE1700) xenon lamp configured at 500 W.m^{-2} in the UV-visible domain (300–800 nm) with an irradiance at 340 nm measured as 0.5 W.m^{-2} [29]. IR irradiation and UV photons below 300 nm were cut off using an Atlas "daylight filter". The black standard temperature (BST) was fixed at 60°C, corresponding to *ca.* 37°C in the irradiation chamber. Further physico-chemical characterizations were performed on samples exposed for 120 h of irradiation at 500 W.m^{-2}.

2.4. Characterization techniques

Proton nuclear magnetic resonance (^{1}H NMR) spectra were recorded in DMSO, using a Bruker AMX-500 spectrometer at a frequency of 500 MHz. Size-exclusion chromatography (SEC) were carried out on an Agilent 1200 apparatus in THF (containing 2wt% of NEt_3). Samples in solution (1 mg.mL^{-1}) were injected with a 1 mL.min^{-1} flow rate at 35°C in a pre-column PL gel 10 mm (50×7.5 mm) followed by two gradient columns PL gel 10 mm mixed-B (300×7.5 mm). Molecular weights and molecular weight distributions were calculated by reference to a relative calibration curve made of polystyrene standards. Thermal gravimetric analyses (TGA) were performed using a TGA Q500 from TA Instruments from room temperature to 800°C, under nitrogen flow at a heating rate of 20°C.min^{-1}. Differential scanning calorimetry (DSC) was performed on a DSC Q200 from TA Instruments using a heat-cool-heat method scanning from -80°C to 80°C at a heating and cooling

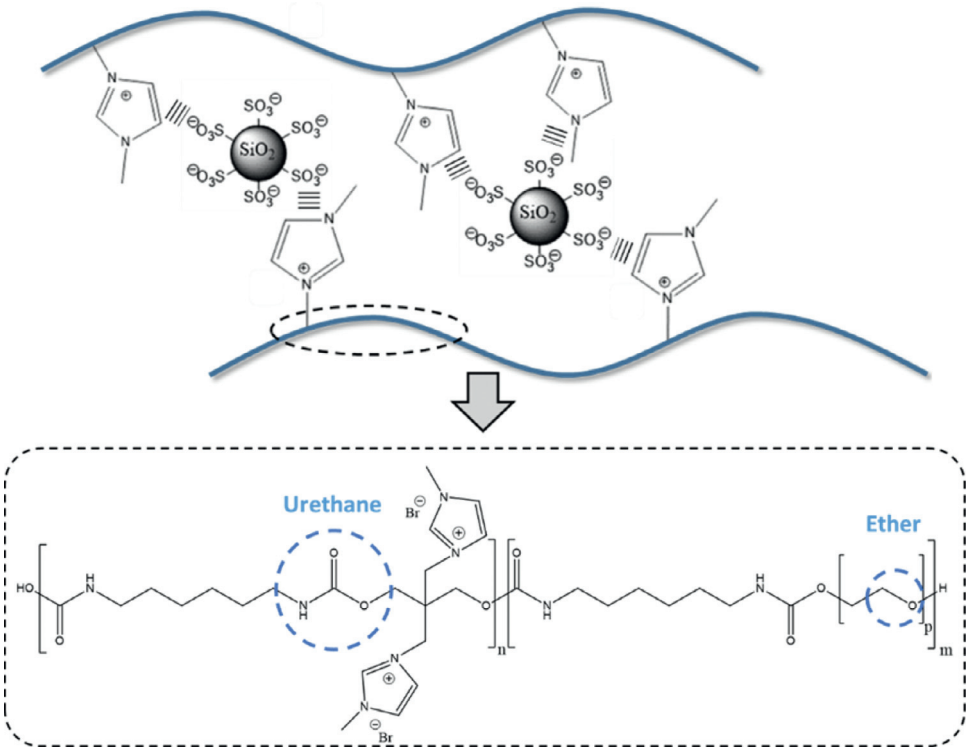

Fig. 1. Ionic nanocomposites synthesized via self-assembly of *im*-PU and SiO_2-SO_3H that leverage Coulomb interactions.

rate of 10°C.min^{-1}. All materials were sputter-coated with gold and then analyzed through scanning electron microscopy (SEM) using a Philips XL20 microscope (1-30kV). Infrared spectra of polymer films were recorded in transmission mode with a Nicolet 6700 FTIR spectrometer, working with OMNIC software. Spectra were obtained using 32 scans and a 4 cm^{-1} resolution. Rheological measurements were made using an Anton Paar Rheometer MCR-302 using a plate-plate geometry system with a 25 mm diameter. Frequency sweep measurements were performed at 60°C with a strain of 1% and a frequency range between 0.1 Hz and 100 Hz. Small-angle X-ray scattering (SAXS) experiments were carried out in the beamline 1W2A at Beijing Synchrotron Radiation Facility (BSRF) [30]. The wavelength of the X-ray radiation was 1.54 Å. The detector was Pilatus 1 M (DECTRIS) containing 981×1043 pixels with a pixel size of 172×172 μm^2. The exposure time was 10 s for each sample and the sample to detector distance was 2862 mm. Intensity profiles were obtained by averaging the two-dimensional (2D) patterns by Fit2D package. Dielectric relaxation measurements were performed on a Broadband Dielectric Spectrometer (Novocontrol Technologies). Samples of 25×25 mm^2 were placed between two gold-plated electrodes (diameter of 20 mm). The complex permittivity $\varepsilon^*(f) = \varepsilon'(f) - i\varepsilon''(f)$, with ε' the storage permittivity and ε'' the loss permittivity, was measured in the frequency range [10^{-1} - 10^6 Hz] using an Alpha Analyzer. Samples were analyzed at different temperatures from -60°C to 60°C with a step of 5°C. Temperature stabilization phase was applied at each temperature step. The β relaxation was fitted with Havriliak-Negami function Eq. (1):

$$\varepsilon* = \varepsilon_\infty + \frac{\varepsilon_0 - \varepsilon_\infty}{(1 + (i\omega\tau_{HN})^{\alpha HN})^{\beta HN}} \quad (1)$$

with ε^* the complex dielectric permittivity, ε_0 and ε_∞ the permittivity at low and high frequency limits respectively, τ_{HN} the relaxation time and α_{HN} and β_{HN} the parameters describing the distribution of relaxation times, *i.e.* respectively the width and asymmetric broadening of the complex dielectric response. Relaxation times τ_{HN} related to β-relaxation were then obtained from the fit of the dielectric loss spectra. Activation energy associated to the β-relaxation times were assigned based on Arrhenius law fitting Eq. (2):

$$\tau_{HN} = \tau_0 e^{-\frac{E_a}{RT}} \quad (2)$$

where τ_{HN} correspond to the relaxation time, τ_0 is the pre-exponent factor, E_a the activation energy, T the temperature and R is the gas constant [31].

3. Results & discussion

3.1. Investigation of photooxidation kinetics

The chemical structure of ionic organic-inorganic hybrids with optimum electrostatic interactions of imidazolium-functionalized poly(ethylene glycol)-based polyurethane (*im*-PU, *ca.* 0.1 mmol.g^{-1} of imidazolium moieties) and surface-modified sulfonate silica nanoparticles (SiO_2-SO_3H, *ca.* 1 mmol.g^{-1} of sulfonate moieties) were schematically shown in Fig. 1. Theoretical charge balance (*i.e.* 1:1 ratio of sulfonate:imidazolium moieties) is herein achieved at 10 wt% of SiO_2-SO_3H to maximize the Coulomb interactions in the system [8,9]. Rheological investigations confirmed the creation of an extensive 3D network of silica nanoparticles within the material at this loading. Neat *im*-PU and ionic *im*-PU/SiO_2-SO_3H hybrid were then irradiated at $\lambda > 300$ nm in the presence of oxygen to elucidate their photodegradation under accelerated ageing conditions. Pristine *im*-PU and *im*-PU/SiO_2-SO_3H materials show no difference in the FTIR spectra with infrared absorption bands at *ca.* 3350, 1720 and 1550 cm^{-1}, respectively corresponding to hydroxyl, carbonyl and nitrogen secondary amine functional groups (*i.e.* N-H, C-N bonds) observed (Fig. S1 in the ESI).

IR spectra of *im*-PU and *im*-PU/SiO_2-SO_3H materials aged in accelerated conditions reveal modifications of their chemical structures, mainly occurring in the hydroxyl (*i.e.* 3500-3000 cm^{-1}) and

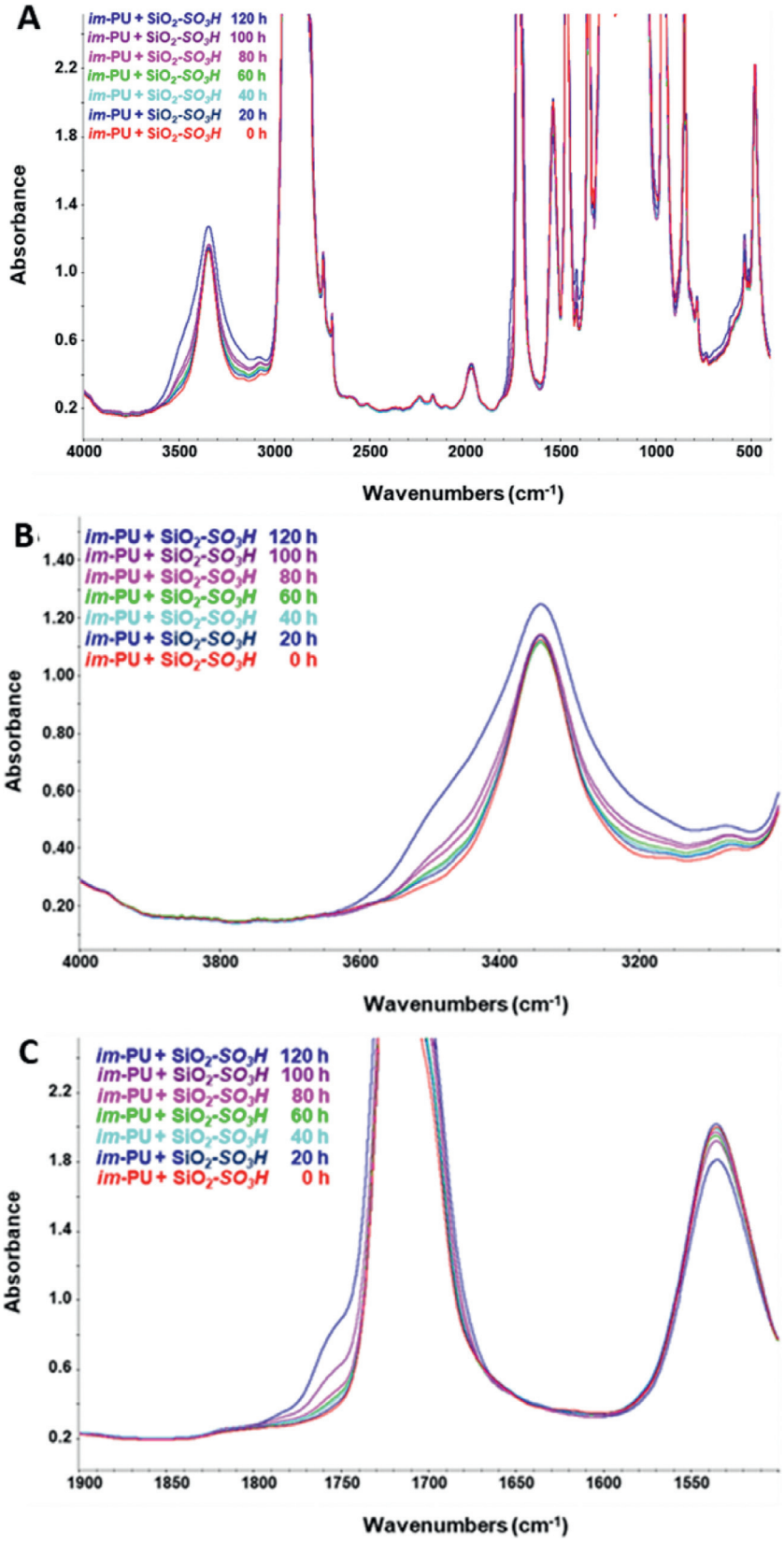

Fig. 2. FTIR spectra of ionic *im*-PU/SiO_2-SO_3H hybrid during photooxidation (A) between 4000 and 400 cm^{-1}, (B) in the hydroxyl region (4000 – 3000 cm^{-1}) and (C) in the carbonyl region (1900 – 1500 cm^{-1}).

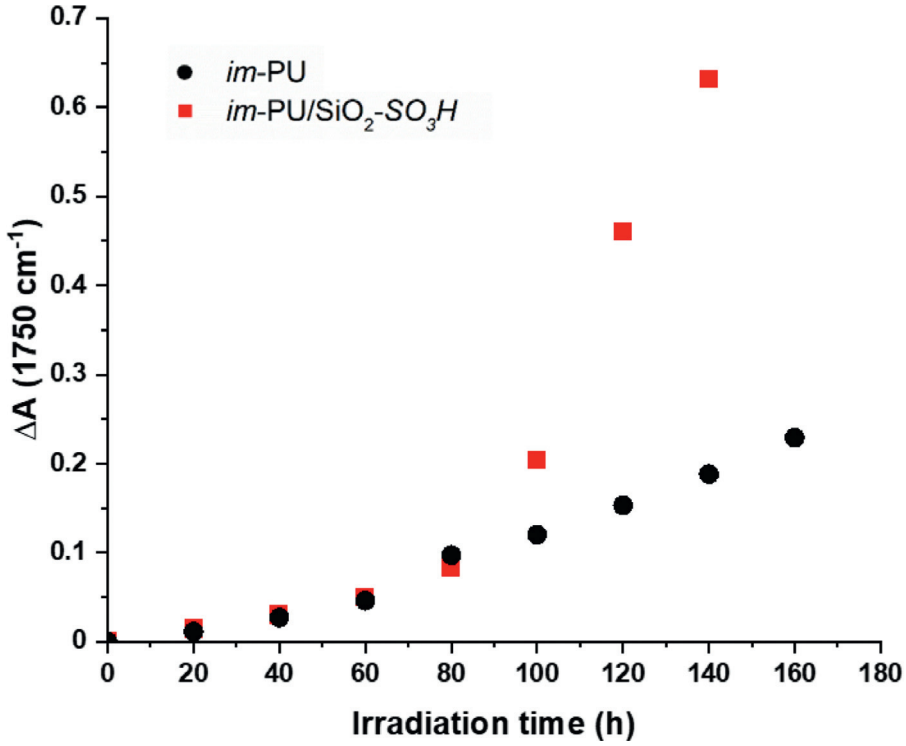

Fig. 3. Variations of absorbance as a function of irradiation time at 1750 cm^{-1} for neat *im*-PU (black, full circle) and ionic *im*-PU/SiO_2-SO_3H hybrid (red, full square) (with correction of thickness).

carbonyl (*i.e.* 1900-1500 cm^{-1}) domains as well as in the fingerprint domain (*i.e.* 1500-800 cm^{-1}) (Fig. 2A and Figure S2A in ESI). A broad band is formed in the hydroxyl region with two absorption maxima at *ca.* 3420 cm^{-1} and *ca.* 3300 cm^{-1} attributed to the formation of new hydrogen-bonded hydroxyls (Fig. 2B and Figure S2B in ESI). Within the carbonyl region, the appearance of a band at *ca.* 1750 cm^{-1} can be assigned to ester functions, which are attributed to the degradation of the polyether backbone of PEG-based *im*-PU segments under photooxidative conditions (Fig. 2C and Figure S2C in ESI). As already described previously, polyethers are known to produce formate under photooxidation (Figure S3 in ESI) [32–34]. However, these oxidation products cannot be observed in IR spectra because the intense absorption band of carbonyl function of urethane is already present in the IR spectra of both samples (*i.e.* *im*-PU and *im*-PU/SiO_2-SO_3H, see Figure S1 in ESI). In contrast, urethane bonds in *im*-PU do not seem to significantly degrade in such accelerated ageing conditions, since oxidative products such as carboxylic acid and primary urethanes are not observed [33]. Finally, the relative increase of the signal at *ca.* 1420 cm^{-1} in the fingerprint domain corresponds to the appearance of carboxylate functional groups, while the signal at *ca.* 1170 cm^{-1} is related to C-O bonds of carbonyl products.

Since esters are the primary oxidation products formed during the photoxidation of neat *im*-PU and ionic *im*-PU/SiO_2-SO_3H hybrid, the kinetic curves of photooxidation are plotted at 1750 cm^{-1}, allowing to compare the oxidation kinetics of both materials (Fig. 3). While *im*-PU and *im*-PU/SiO_2-SO_3H materials have similar oxidation kinetics at short exposure times, the ionic *im*-PU/SiO_2-SO_3H hybrid is more rapidly degraded from *ca.* 100h of irradiation under photooxidative conditions. The latter results suggest that the addition of SiO_2-SO_3H nanoparticles within *im*-PU have a degrading effect on the polymer photooxidation. This effect may be likely attributed to the organic-inorganic nature of the hybrid (*i.e.* silica being a prodegrading agent) or to a lesser extent the surface functionalization of the nanoparticles.

3.2. Age-related changes in macromolecular architecture

Changes in molecular weight and molecular weight distribution during the photooxidation of neat *im*-PU and ionic *im*-PU/SiO_2-SO_3H hybrid are followed by SEC. While the molecular weight of neat *im*-PU decrease from *ca.* 58 000 $g.mol^{-1}$ to *ca.* 30 000 $g.mol^{-1}$ after 120h of irradiation under photooxidative conditions, a very dramatic drop in molecular weight together with a broader molecular weight distribution ($M_n \sim 1\ 000\ g.mol^{-1}$; $Đ \sim 2.6$) are recorded for the ionic *im*-PU/SiO_2-SO_3H hybrid (Table 1). This reveals chain scissions that can be correlated to the formation of formate functional groups under photooxidation [32–34]. Molecular weight decrease in the ionic hybrid is attributed to faster degradation of the *im*-PU backbone under photooxidative conditions. Although FTIR signatures of either imidazolium or sulfonate species are not discernible within the fingerprint region, ^{1}H NMR analyses are performed to further investigate changes in the electrostatic imidazolium-sulfonate interactions that are involved in the ionic *im*-PU/SiO_2-SO_3H hybrid (Figure S4 in ESI). While protons (^{1}H-NMR in $CDCl_3$) in the 8-10 ppm region (δ = 8.96, 9.21 and 9.77 ppm in Figure S4 in ESI) confirmed the incorporation of cationic imidazolium rings into the *im*-PU backbone, the signals disappear entirely after the photooxidation of neat *im*-PU. In contrast, adding SiO_2-SO_3H nanoparticles in *im*-PU to generate the ionic *im*-PU/SiO_2-SO_3H hybrid readily allow preserving the imidazolium protons through photochemical ageing. The proximity of the cationic imidazolium rings to the anionic sulfonate groups along with maximizing Coulomb interactions is thought to protect the resulting ionic crosslinks from photodegradation. The latter results further suggest that the dynamic and reversible nature of ionic bonding present in the system are not affected by the photooxidative ageing.

The photodegradation which results in polymer chain breaking is known to directly affect the thermal properties and crystallinity of materials [35]. Herein, a drop of melting (T_m) and crys-

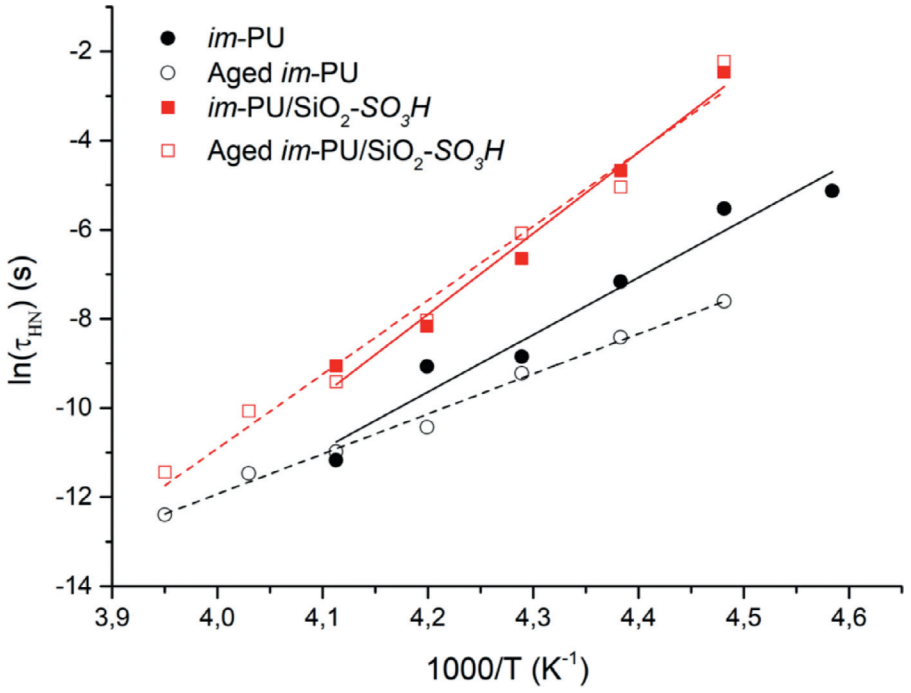

Fig. 4. Evolution of relaxation times over temperature for unaged *im*-PU (black, full circle), unaged ionic *im*-PU/SiO_2-SO_3H hybrid (red, full square), aged *im*-PU (black, open circle) and aged ionic *im*-PU/SiO_2-SO_3H hybrid (red, open square).

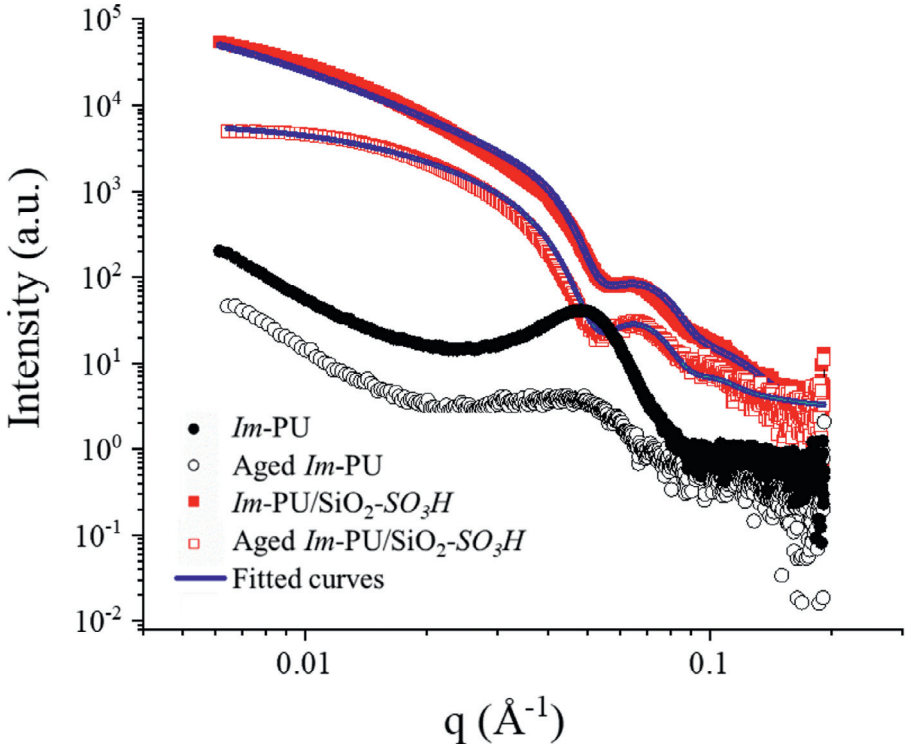

Fig. 5. Small Angle X-Ray Scattering (SAXS) profiles of unaged *im*-PU (black, full circle), unaged ionic *im*-PU/SiO_2-SO_3H hybrid (red, full square), aged *im*-PU (black, open circle) and aged ionic *im*-PU/SiO_2-SO_3H hybrid (red, open square).

tallization (T_c) temperatures together with an increase of crystallization enthalpy are clearly observed for the aged *im*-PU and *im*-PU/SiO_2-SO_3H materials (Table 1 and Figure S5 in ESI). When radical mechanisms are involved, random chain scission and crosslinking often compete. Thought, the main degradation mechanism is herein attributed to random chain scission, leading to the formation of fractions of the polymer with shorter chains, which have a greater capacity to form an ordered phase. Although the thermal stability of neat *im*-PU does not seem to be affected by the photooxidation, TGA measurements reveal that the ionic *im*-PU/SiO_2-SO_3H hybrid degrades at somewhat lower temperature and shows lower residual fraction owing to inhomogeneous distribution of sil-

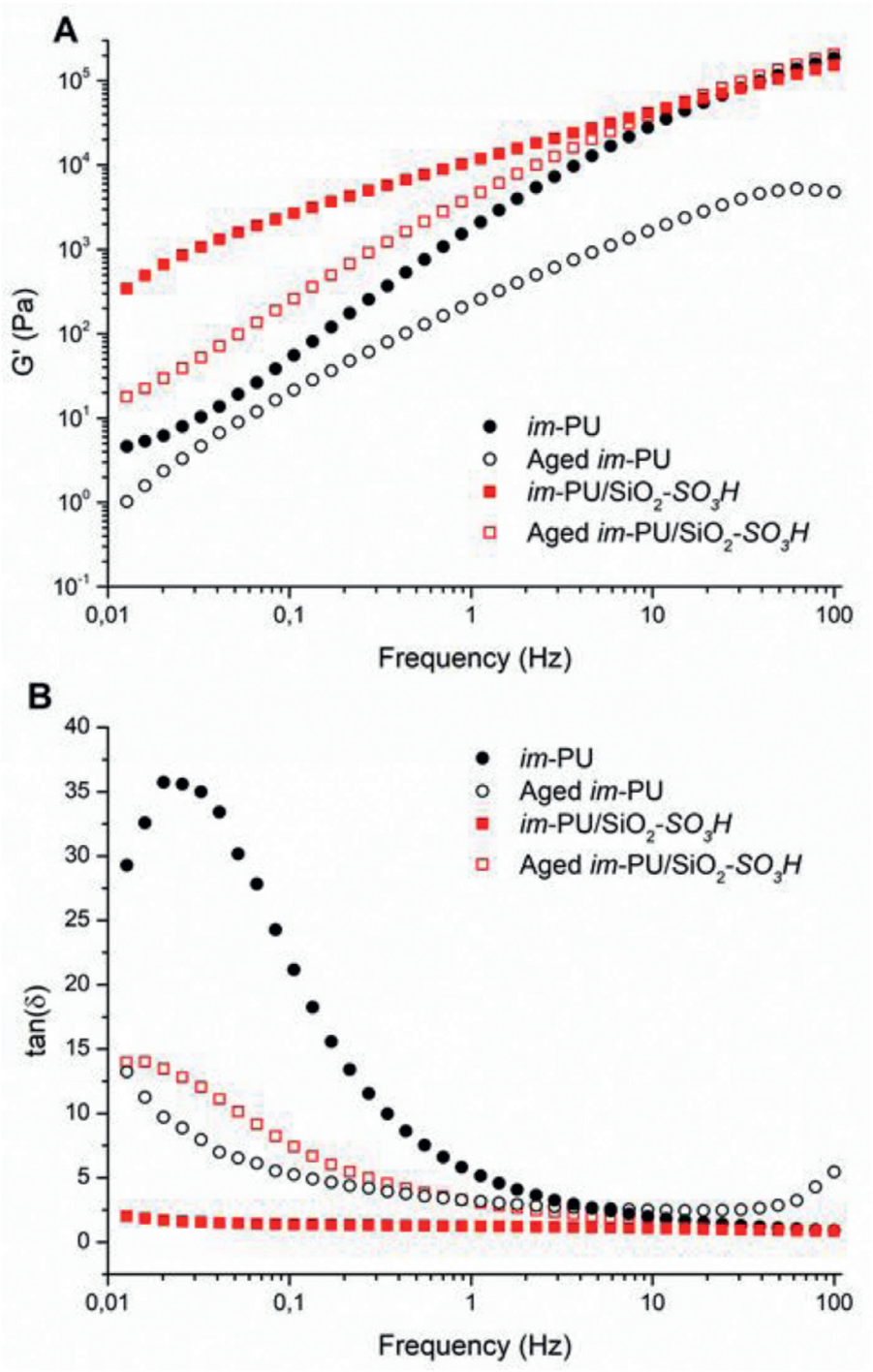

Fig. 6. Storage modulus G' (A) and loss factor Tanδ (B) of unaged *im*-PU (black, full circle), unaged ionic *im*-PU/SiO_2-SO_3H hybrid (red, full square), aged *im*-PU (black, open circle) and aged ionic *im*-PU/SiO_2-SO_3H hybrid (red, open square).

Table 1
Molecular weights and thermal properties of unaged *im*-PU, unaged ionic *im*-PU/SiO_2-SO_3H hybrid, aged *im*-PU and aged ionic *im*-PU/SiO_2-SO_3H hybrid (*i.e.* at 500 W.m^{-2}, 120h).

	M_n[g.mol^{-1}]	M_w[g.mol^{-1}]	Đ	T_c[°C]	T_m[°C]	ΔH_c[J.g^{-1}]
im-PU	58 000	108 000	1.9	19.8	43.1	71
im-PU/SiO_2-SO_3H	58 000	108 000	1.9	22.8	43.4	64
Aged im-PU	30 000	64 000	2.1	16.8	41.5	88
Aged im-PU/SiO_2-SO_3H	1 000	3 000	2.6	1.6	39.2	84

M_n: Number average molecular weight; M_w: Weight average molecular weight;
Đ: polydispersity; T_c: Crystallization temperature; T_m: Melting temperature;
ΔH_c: Crystallization enthalpy.

ica nanoparticles (*i.e.* leading to fractions of varying agglomeration states) after ageing (Figure S6 in ESI). While a two-step degradation is recorded, the weight losses are attributed to thermal degradation of urethane (at *ca.* 300°C) and ether (at *ca.* 400°C) bonds of the PEG-based *im*-PU segments. The resulting thermal behavior changes are attributed to severe chain scissions into the *im*-PU backbone in the presence of SiO_2-SO_3H nanoparticles.

In addition, the mechanical behavior of neat *im*-PU and ionic *im*-PU/SiO_2-SO_3H hybrid dramatically changes, when exposed to photooxidative conditions (Figure S7 in ESI). The most striking feature concerns the ionic *im*-PU/SiO_2-SO_3H hybrid, which displays very limited plastic deformation and inherent brittleness, so that DMTA cannot be adequately performed. In contrast, DMTA measurements of neat *im*-PU reveal a drop in both storage and loss modulus as well as broader loss factor after ageing. Besides, the α-transition shifts to higher temperature since crosslinking reactions are involved upon aging [36]. Additional dielectric spectroscopy measurements readily allow monitoring not only of the α-relaxation but also β-relaxation processes (Figure S8 in ESI). While the α-relaxation most commonly refers to large scale rearrangement of *im*-PU chains, the β-relaxation is associated to segmental motions from the amorphous *im*-PU chains [37,38]. The α-process is no longer observed after ageing, because the conducting contributions overlap with the α-relaxation [39]. Using Havriliak-Negami and Arrhenius law fittings (see experimental section), the characteristic relaxation time and activation energy for the β-transition were determined (Fig. 4). A good overview of dynamic properties is given by the activation energy, which is herein proportional to the energy required to break and reform the ionic imidazolium-sulfonate interactions [40]. Although the activation energies of neat *im*-PU and ionic *im*-PU/SiO_2-SO_3H hybrid decrease from 107 kJ.mol^{-1} to 75 kJ.mol^{-1} and from 151 kJ.mol^{-1} to 138 kJ.mol^{-1} respectively, after ageing, the corresponding relaxation times are at most on the same order of magnitude. Unlike the α-relaxation, effects of the photochemical ageing on the β-relaxation process are obviously very limited [41,42].

3.3. Age-related changes in morphological & rheological properties

SEM measurements show the ionic *im*-PU/SiO_2-SO_3H hybrid to be well-dispersed, a typical challenge of conventional nanocomposites, that we attributed to the presence of electrostatic imidazolium-sulfonate interactions in the system [8,9,43]. While the morphology of neat *im*-PU does not seem to be affected during the photochemical ageing, the ionic *im*-PU/SiO_2-SO_3H hybrid tends to form silica nanoparticles aggregates after ageing (Figure S9 in ESI). SAXS experiments are further performed to measure the level of dispersion of SiO_2-SO_3H nanoparticles within the *im*-PU matrix (Fig. 5). Neat *im*-PU shows a maximum intensity at 0.049 Å^{-1} corresponding to the long period of *im*-PU lamellar crystals. The long period of neat *im*-PU is calculated to be *ca.* 12.8 nm from Bragg's law ($Lp = 2\pi/q_{max}$) [44], and it does not change under photooxidative conditions. On the other hand, the scattering peak for the aged *im*-PU is broader and lower, suggesting a decrease in crystallinity. Adding ionic SiO_2-SO_3H nanoparticles into *im*-PU to generate the ionic *im*-PU/SiO_2-SO_3H hybrid leads to greater intensity due to the higher scattering contrast between the nanoparticles and the polymer matrix. As shown in our previous study [43], the SAXS profiles of the *im*-PU/SiO_2-SO_3H hybrid cannot be fitted by the sphere form factor but can rather be fitted by polydisperse spheres with a structure factor of sticky hard sphere considering the particles have an attractive potential. The fitting allows extracting an average radius of silica nanoparticles of 80 Å with a polydispersity of 0.12 assuming a Gaussian size distribution, which is consistent with the particle size distribution of silica nanoparticles (*ca.* 17 ± 5 nm of diameter). There are small differences between the SAXS profiles of pristine and aged ionic *im*-PU/SiO_2-SO_3H nanocomposites, especially in the low q region, indicating different dispersion states of the nanoparticles in the hybrids. However, SEM results clearly suggest the existence of particle aggregates well beyond 100 nm after ageing (see Figure S9 in ESI). Because the size of those aggregates in the aged is beyond the detection limit of conventional SAXS, it is not possible to make statements about the global morphology of the nanoparticles in the hybrids by SAXS. Still, the fitting results further indicate that the depth of the attractive potential well for the ionic hybrid decrease from 4.6 kT to 4.0 kT (at a fixed thickness of 1.6 Å, *i.e.* the smallest allowable) after aging, suggesting that the ionic interactions between the particles are weaker after aging.

Rheologically, the storage modulus increases by several orders of magnitude at low frequencies upon the addition of SiO_2-SO_3H into *im*-PU to form the ionic hybrid (Fig. 6). Using the Winter-Chambon criterion of the loss factor tan(δ) being frequency independent, we find that the ionic *im*-PU/SiO_2-SO_3H hybrid led to the creation of an extensive 3D network of silica nanoparticles within the material [45]. As expected, a significant decrease in storage modulus is seen, when both *im*-PU and *im*-PU/SiO_2-SO_3H materials are exposed to photooxidative conditions (Fig. 6A). The most striking feature concerns the frequency-independent gel-point evaluation of the ionic *im*-PU/SiO_2-SO_3H hybrid, which transition to weaker gel-like behavior after ageing (Fig. 6B). Although electrostatic imidazolium-sulfonate interactions are likely preserved in the system, we believe that the degradation of the *im*-PU backbone under photooxidative conditions led to the partial alteration of the extensive 3D particle network within the ionic *im*-PU/SiO_2-SO_3H hybrid.

4. Conclusions

The photodegradation process of organic-inorganic hybrids, which integrate the reversible nature of electrostatic interactions present in ionic systems with the reinforcement ability of nanoparticles in nanocomposites was studied. Ionic hybrid materials made of a combination of imidazolium-functionalized poly(ethylene glycol)-based polyurethane (*im*-PU) and surface-modified sulfonate silica nanoparticles (SiO_2-SO_3H) were studied before and after accelerated ageing conditions. Under accelerated photooxidative conditions, the addition of SiO_2-SO_3H nanoparticles in *im*-PU matrix led to faster photooxidative degradation. Overall, the silica nanoparticles are responsible for the photodegradation rather than the presence of ionic interactions in the system. Although electrostatic imidazolium-sulfonate interactions are likely preserved in the system, the degradation of the polyether backbone of *im*-PU chains under photooxidative conditions led to the partial alteration of the extensive 3D particle network within the ionic *im*-PU/SiO_2-SO_3H hybrid. In addition, the mechanical behavior and thermal stability of neat *im*-PU and ionic *im*-PU/SiO_2-SO_3H hybrid dramatically change, when exposed to photooxidative conditions. The most striking feature concerns the ionic *im*-PU/SiO_2-SO_3H hybrid which displays very limited plastic deformation and inherent brittleness after ageing. Although the morphology of the pristine ionic hybrid is consistent with maximizing electrostatic interactions between cationic imidazolium rings on *im*-PU chains and anionic sulfonate groups on the silica, the ionic *im*-PU/SiO_2-SO_3H hybrids tend to form silica nanoparticles aggregates during photochemical ageing. SAXS profiles further support the age-related aggregation of silica nanoparticles along the degradation of the *im*-PU backbone under photooxidative conditions. The present contribution provides a deeper understanding about the photochemical ageing process, which can be of real value in designing materials for various applications.

Declaration of Competing Interest

The authors declare that they have no known competing financial interests or personal relationships that could have appeared to influence the work reported in this paper.

CRediT authorship contribution statement

J.-E. Potaufeux: Investigation, Writing – original draft. **G. Rapp:** Investigation. **S. Barrau:** Investigation. **G. Liu:** Investigation, Methodology. **C. Zhang:** Investigation. **Emmanuel P. Giannelis:** Resources, Conceptualization, Writing – review & editing. **D. Notta-Cuvier:** Investigation, Methodology. **F. Lauro:** Investigation, Methodology. **J.-M. Raquez:** Project administration, Conceptualization. **J. Odent:** Supervision, Writing – review & editing. **S. Therias:** Validation, Writing – review & editing.

Acknowledgments

The authors gratefully acknowledge support from both the Wallonia and the European Commission “FSE and FEDER” in the frame of LCFM-BIOMASS project as well as the National Fund for Scientific Research (F.R.S.-FNRS). We would like to thank the financial support provided by the BIODEST project. This project has received funding from the European Union’s Horizon 2020 research and innovation program under the Marie Sklodowska-Curie grant agreement no. 778092. LAMIH authors are grateful to CISIT, the Hauts de France Region, the European Community, the Regional Delegation for Research and Technology, the Ministry of Higher Education and Research and the National Center for Scientific Research for their financial support. J.-M. Raquez is ‘Maître de Recherches’ by the F.R.S.-F.N.R.S.

Supplementary materials

Supplementary material associated with this article can be found, in the online version, at doi:10.1016/j.polymdegradstab.2022.109872.

References

[1] S.C. Grindy, R. Learsch, D. Mozhdehi, J. Cheng, D.G. Barrett, Z. Guan, P.B. Messersmith, N. Holten-Andersen, Control of hierarchical polymer mechanics with bioinspired metal-coordination dynamics, Nature Mater. 14 (12) (2015) 1210–1216.
[2] J. Liu, S. Zhang, L. Zhang, L. Liu, Y. Bai, Uniaxial stretching of polylactide with different initial crystalline morphologies and temperature effect, Eur. Polym. J. 61 (2014) 83–92.
[3] T.L. Sun, T. Kurokawa, S. Kuroda, A.B. Ihsan, T. Akasaki, K. Sato, M.A. Haque, T. Nakajima, J.P. Gong, Physical hydrogels composed of polyampholytes demonstrate high toughness and viscoelasticity, Nature Mater. 12 (10) (2013) 932–937.
[4] J.-E. Potaufeux, J. Odent, D. Notta-Cuvier, F. Lauro, J.-M. Raquez, A comprehensive review of the structures and properties of ionic polymeric materials, Polym. Chem. 11 (37) (2020) 5914–5936.
[5] W. Wang, Y. Zhang, W. Liu, Bioinspired fabrication of high strength hydrogels from non-covalent interactions, Prog. Polym. Sci. 71 (2017) 1–25.
[6] S. Nkhwa, E. Kemal, N. Gurav, S. Deb, Dual polymer networks: a new strategy in expanding the repertoire of hydrogels for biomedical applications, J. Mater. Sci. 30 (10) (2019) 114.
[7] T. Yuan, X. Cui, X. Liu, X. Qu, J. Sun, Highly Tough, Stretchable, Self-Healing, and Recyclable Hydrogels Reinforced by in Situ-Formed Polyelectrolyte Complex Nanoparticles, Macromolecules 52 (8) (2019) 3141–3149.
[8] J. Odent, J.M. Raquez, P. Dubois, E.P. Giannelis, Ultra-stretchable ionic nanocomposites: from dynamic bonding to multi-responsive behavior, J. Mater. Chem. A 5 (26) (2017) 13357–13363.
[9] J.-E. Potaufeux, J. Odent, D. Notta-Cuvier, R. Delille, S. Barrau, E.P. Giannelis, F. Lauro, J.-M. Raquez, Mechanistic insights on ultra-tough polylactide-based ionic nanocomposites, Compos. Sci. Technol. (2020) 108075.
[10] S.L. Banerjee, T. Swift, R. Hoskins, S. Rimmer, N.K. Singha, A muscle mimetic polyelectrolyte–nanoclay organic–inorganic hybrid hydrogel: its self-healing, shape-memory and actuation properties, J. Mater. Chem. B 7 (9) (2019) 1475–1493.
[11] M. Zhong, Y.-T. Liu, X.-M. Xie, Self-healable, super tough graphene oxide–poly(acrylic acid) nanocomposite hydrogels facilitated by dual cross-linking effects through dynamic ionic interactions, J. Mater. Chem. B 3 (19) (2015) 4001–4008.
[12] J.-L. Gardette, A. Rivaton, S. Therias, Photodegradation processes in polymeric materials, in: Photochemistry and Photophysics of Polymer Materials, John Wiley & Sons, Inc., Hoboken, NJ, USA, 2010, pp. 569–601.
[13] D. Cangialosi, V.M. Boucher, A. Alegría, J. Colmenero, Physical aging in polymers and polymer nanocomposites: recent results and open questions, Soft Matter 9 (36) (2013) 8619.
[14] D.S. Jacobs, S.-R. Huang, Y.-L. Cheng, S.A. Rabb, J.M. Gorham, P.J. Krommenhoek, L.L. Yu, T. Nguyen, L. Sung, Surface degradation and nanoparticle release of a commercial nanosilica/polyurethane coating under UV exposure, J Coat Technol Res 13 (5) (2016) 735–751.
[15] L. Sung, D. Stanley, J.M. Gorham, S. Rabb, X. Gu, L.L. Yu, T. Nguyen, A quantitative study of nanoparticle release from nanocoatings exposed to UV radiation, J Coat Technol Res 12 (1) (2015) 121–135.
[16] T. Nguyen, B. Pellegrin, C. Bernard, S. Rabb, P. Stuztman, J.M. Gorham, X. Gu, L.L. Yu, J.W. Chin, Characterization of surface accumulation and release of nanosilica during irradiation of polymer nanocomposites by ultraviolet light, J Nanosci Nanotechnol 12 (8) (2012) 6202–6215.
[17] R. Watanabe, A. Sugahara, H. Hagihara, K. Sakamoto, Y. Nakajima, Y. Naganawa, Polypropylene-based nanocomposite with enhanced aging stability by surface grafting of Silica Nanofillers with a silane coupling agent containing an antioxidant, ACS Omega 5 (21) (2020) 12431–12439.
[18] S. Amanuel, A.N. Gaudette, S.S. Sternstein, Enthalpic relaxation of silica-polyvinyl acetate nanocomposites, J. Polym. Sci., Part B: Polym. Phys. 46 (24) (2008) 2733–2740.
[19] A.L. Flory, T. Ramanathan, L.C. Brinson, Physical aging of single wall carbon nanotube polymer nanocomposites: effect of functionalization of the nanotube on the enthalpy relaxation, Macromolecules 43 (9) (2010) 4247–4252.
[20] G. Cheraghian, M.P. Wistuba, Ultraviolet aging study on bitumen modified by a composite of clay and fumed silica nanoparticles, Sci. Rep. 10 (1) (2020) 11216.
[21] S. Morlat, B. Mailhot, D. Gonzalez, J.-L. Gardette, Photo-oxidation of polypropylene/montmorillonite nanocomposites. 1. Influence of Nanoclay and Compatibilizing agent, Chem. Mater. 16 (3) (2004) 377–383.
[22] G.A.M. Falcão, T.G. Almeida, M.A.G. Bardi, L.H. Carvalho, E.L. Canedo, PBAT/organoclay composite films—part 2: effect of UV aging on permeability, mechanical properties and biodegradation, Polym. Bull. 76 (1) (2019) 291–301.
[23] D. Cangialosi, V.M. Boucher, A. Alegría, J. Colmenero, Enhanced physical aging of polymer nanocomposites: the key role of the area to volume ratio, Polymer 53 (6) (2012) 1362–1372.
[24] Y. Guo, C. Zhang, C. Lai, R.D. Priestley, M. D’Acunzi, G. Fytas, Structural relaxation of polymer nanospheres under soft and hard confinement: isobaric *versus*Isochoric conditions, ACS Nano 5 (7) (2011) 5365–5373.
[25] S.E. Harton, S.K. Kumar, H. Yang, T. Koga, K. Hicks, H. Lee, J. Mijovic, M. Liu, R.S. Vallery, D.W. Gidley, Immobilized polymer layers on spherical nanoparticles, Macromolecules 43 (7) (2010) 3415–3421.
[26] J. Berriot, H. Montes, F. Lequeux, D. Long, P. Sotta, Evidence for the shift of the glass transition near the particles in silica-filled elastomers, Macromolecules 35 (26) (2002) 9756–9762.
[27] A.K. Łasińska, M. Marzantowicz, J.R. Dygas, F. Krok, Z. Florjańczyk, A. Tomaszewska, E. Zygadło-Monikowska, Z. Żukowska, U. Lafont, Study of ageing effects in polymer-in-salt electrolytes based on poly(acrylonitrile-co-butyl acrylate) and lithium salts, Electrochimica Acta 169 (2015) 61–72.
[28] H. Akimoto, T. Kanazawa, M. Yamada, S. Matsuda, G.O. Shonaike, A. Murakami, Impact fracture behavior of ethylene ionomer and structural change after stretching, J. Appl. Polym. Sci. 81 (7) (2001) 1712–1720.
[29] A. Perthué, T. Gorisse, H.Santos Silva, D. Bégué, A. Rivaton, G. Wantz, Influence of traces of oxidized polymer on the performances of bulk heterojunction solar cells, Mater. Chem. Front. 3 (8) (2019) 1632–1641.
[30] Z. Li, Z. Wu, G. Mo, X. Xing, P. Liu, A Small-Angle X-Ray scattering station at beijing synchrotron radiation facility, Instrument Sci Technol 42 (2) (2014) 128–141.
[31] C.-Y. Liu, J. He, R. Keunings, C. Bailly, New linearized relation for the universal viscosity−temperature behavior of polymer melts, Macromolecules 39 (25) (2006) 8867–8869.
[32] S. Morlat, J.-L. Gardette, Phototransformation of water-soluble polymers. I: photo- and thermooxidation of poly(ethylene oxide) in solid state, Polymer 42 (14) (2001) 6071–6079.
[33] C. Wilhelm, J.-L. Gardette, Infrared analysis of the photochemical behaviour of segmented polyurethanes: aliphatic poly(ether-urethane)s, Polymer 39 (24) (1998) 5973–5980.
[34] F. Hassouna, S. Morlat-Therias, G. Mailhot, J.-L. Gardette, Influence of water on the photodegradation of poly(ethylene oxide), Polymer Degradat Stab - Polym Degrad Stabil 92 (2007) 2042–2050.
[35] E. Olewnik-Kruszkowska, Effect of UV irradiation on thermal properties of nanocomposites based on polylactide, J. Therm. Anal. Calorim. 119 (1) (2015) 219–228.
[36] Y. Du, J. Zheng, G. Yu, Influence of thermally-accelerated aging on the dynamic mechanical properties of HTPB coating and crosslinking density-modified model for the payne effect, Polymers 12 (2) (2020) 403.
[37] T. Körber, F. Mohamed, M. Hofmann, A. Lichtinger, L. Willner, E.A. Rössler, The nature of secondary relaxations: the case of Poly(ethylene- *alt*-propylene) studied by dielectric and deuteron NMR spectroscopy, Macromolecules 50 (4) (2017) 1554–1568.

[38] Y. Ding, S. Pawlus, A.P. Sokolov, J.F. Douglas, A. Karim, C.L. Soles, Dielectric spectroscopy investigation of relaxation in C_{60}−Polyisoprene nanocomposites, Macromolecules 42 (8) (2009) 3201–3206.
[39] K. Se, K. Adachi, T. Kotaka, Dielectric relaxations in Poly(ethylene oxide): dependence on molecular weight, Polymer J. 13 (11) (1981) 1009–1017.
[40] P.C. Suarez-Martinez, P. Batys, M. Sammalkorpi, J.L. Lutkenhaus, Time–temperature and time–water superposition principles applied to Poly(allylamine)/Poly(acrylic acid) complexes, Macromolecules 52 (8) (2019) 3066–3074.
[41] E. Muzeau, G. Vigier, R. Vassoille, Physical aging phenomena in an amorphous polymer at temperatures far below the glass transition, J. Non-Crystalline Solids 172-174 (1994) 575–579.
[42] A. Wypych, E. Duval, G. Boiteux, J. Ulanski, L. David, G. Seytre, A. Mermet, I. Stevenson, M. Kozanecki, L. Okrasa, Physical aging of atactic polystyrene as seen by dielectric relaxational and low-frequency vibrational Raman spectroscopies, J. Non-Crystalline Solids 351 (33-36) (2005) 2593–2598.
[43] J.-E. Potaufeux, J. Odent, D. Notta-Cuvier, S. Barrau, C. Magnani, R. Delille, C. Zhang, G. Liu, E.P. Giannelis, A.J. Müller, F. Lauro, J.-M. Raquez, Mastering superior performance origins of ionic Polyure-thane/Silica hybrids, ACS Appl. Polymer Mater. (2021), doi:10.1021/acsapm.1c01396.
[44] N.-D. Tien, T.-P. Hoa, M. Mochizuki, K. Saijo, H. Hasegawa, S. Sasaki, S. Sakurai, Higher-order crystalline structures of poly(oxyethylene) in poly(d,l-lactide)/poly(oxyethylene) blends, Polymer 54 (17) (2013) 4653–4659.
[45] N.J. Fernandes, T.J. Wallin, R.A. Vaia, H. Koerner, E.P. Giannelis, Nanoscale Ionic Mater. Chem. Mater. 26 (1) (2014) 84–96.